Correlation of Hydrogenated Nanocrystalline Silicon Microstructure and Solar Cell Performance

Keda Wang, Anthony Canning, J.R.Weinberg-Wolf, E.C.T. Harley, and Daxing Han
Department of Physics & Astronomy, University of North Carolina at Chapel Hill,
Chapel Hill, NC 27599-3255
Baojie Yan, Guozhen Yue, Jeffrey Yang, and Subhendu Guha
United Solar Ovonic Corporation., 1100 W Maple Road, Troy, MI 48084

ABSTRACT

We used Raman and photoluminescence (PL) spectroscopy to study the relationship between the material properties and the solar cell performance of hydrogenated nanocrystalline silicon (nc-Si:H). The crystalline volume fraction (f_c) was deduced from the Raman spectrum. Generally, a high f_c leads to a high short circuit current density and a low open circuit voltage. PL spectra were measured using 632.8-nm and 442-nm laser lines. There are two distinguished PL peaks at 80 K, one at ~1.4 eV originating from the amorphous region, while the other at ≤ 0.9 eV from the nanocrystalline grain boundary regions. Generally, the intensity fraction of this low energy PL peak, $I_{PLc}/(I_{PLa}+I_{PLc})$, was larger for 442-nm than 632.8-nm excitation, indicating an increase in crystallinity along the growth direction. However, for the best initial performance cells obtained by H_2 dilution profiling and the *i/p* buffer layer, the intensity fraction $I_{PLc}/(I_{PLa}+I_{PLc})$ decreased from the bulk to the top *i/p* interface. The Raman and PL results give insight into the correlation between the microstructures and the cell performance, and verified that properly-controlled crystallinity in the intrinsic layer and buffer layer at the *i/p* interface layer are important for optimizing nc-Si:H solar cells.

INTRODUCTION

Hydrogenated amorphous silicon (a-Si:H) solar panels have been used for both terrestrial and space applications. One limitation of such panels is the light-induced degradation caused by the metastability of a-Si:H. Although much effort has been made to optimize solar cell structures, such as using a spectrum splitting triple-junction structure [1,2], the light-induced degradation still exists in a-Si:H based solar cells. In order to make high efficiency and high stable thin film solar cell, hydrogenated nanocrystalline silicon (nc-Si:H) solar cell has received a great deal of attention in the last decade due to its lower light-induced degradation and higher current density than a-Si:H cell [3-6]. Initial efficiencies of over 10% for a single-junction nc-Si:H solar cell and over 14% for a-Si:H/nc-Si:H double-junction solar cell have been reported [5]. At United Solar, several techniques have been used to increase the deposition rate and improve cell performance [6]. It is well accepted that a high quality material is essential for achieving high efficiency solar cells. Therefore, it is very important to find a direct correlation between material properties and device performance for improving cell efficiency.

In previous studies [7-12], Raman and photoluminescence (PL) spectroscopy have been used to characterize the microstructure and electronic states in nc-Si:H materials and solar cells. The Raman transverse optical (TO) mode was used to deduce the crystalline volume fraction (f_c) [7,8]. For the photoluminescence (PL) spectra of nc-Si:H, a relatively narrow band at low energy was found to be the characteristic peak of nc-Si:H. To distinguish this low energy peak from the defect peak in conventional a-Si:H materials, we measured the temperature dependence

of PL from 15 K to 300 K [9] and found that both the intensity and the peak energy position of the low energy PL peak in nc-Si:H are higher at low temperatures than at high temperatures. This behavior is in contrast to the defect peak in a-Si:H where the defect PL has a weak temperature dependence and is undetectable at low temperatures. In nc-Si:H, when the temperature was increased from 15 to 180 K, the intensity of the nanocrystalline related peak was rapidly quenched, and the peak energy shifted from 1.0 eV to 0.83 eV [9]. Above 180 K, the defect peak appeared and overlapped with the PL from grain boundary regions. The behavior of the low energy PL peak in nc-Si:H was explained in terms of the carrier thermalization in an exponential band tail in the grain boundary region [7,9-11]. The tail width kT_0 was found to be 20-24 meV, which is about half the value in typical a-Si:H.

In this work, we use the same techniques to study the relationship between the material properties and the device performance of nc-Si:H solar cells made using radio frequency (RF), modified very high frequency (MVHF), and microwave (μW) glow discharge. In addition, not only 632.8-nm but also 442-nm laser lines are used for PL excitation to distinguish the difference in electronic density of states between the top layer and bulk.

EXPERIMENTAL AND RESULTS

Several *n-i-p* nc-Si:H solar cells were deposited on Ag/ZnO back reflector using various techniques at different deposition rates. Indium-tin-oxide (ITO) dots with an active area of 0.25 cm^2 were deposited on the *p* layer as the top contact. Current density versus voltage (J-V) characteristics was measured under an AM1.5 solar simulator at 25 °C. Quantum efficiency was measured from 300 nm to 1000 nm to calibrate the short-circuit current density (J_{sc}). Table I summarizes the solar cell deposition conditions and J-V characteristics. Raman measurements were made directly on the solar cells under the ambient condition using the 514.5-nm line from

Table I. Preparation conditions and solar cell performance of the nc-Si:H solar cells studied.

Dep. method	Sample ID#	d (μm)	Rate (Å/s)	Eff (%)	J_{sc} (mA/cm^2)	V_{oc} (V)	FF	Comments
RF	13917	1.1	1	6.66	23.43	0.472	0.593	Flat H_2 dilution, ambient stable
	14085	1.0	1	7.00	22.55	0.493	0.630	**H_2 dilution profiling**, ambient stable
VHF	11667	1.1	3	6.85	23.73	0.464	0.622	Flat H_2 dilution, **thick *i/p* buffer**, ambient stable
	10973	0.9	3	4.92	22.39	0.415	0.530	Flat H_2 dilution, ambient stable
	10976	1.1	3	5.00	23.26	0.406	0.530	Flat H_2 dilution, ambient unstable
	11538	1.1	3	4.55	24.92	0.406	0.450	Flat H_2 dilution, ambient stable
	11486	0.7	12	3.20	17.05	0.381	0.493	Flat H_2 dilution, ambient unstable
μW	7073	0.8	20	3.03	15.22	0.390	0.510	Flat H_2 dilution, ambient stable

an argon-ion laser. The penetration depth of the 514.5-nm light is ~60 nm for a-Si:H and is

larger for nc-Si:H. Figure 1 shows the Raman spectra of the TO mode for the eight cells listed in Table I. The PL spectra for the same samples were measured in a temperature range of 80-300 K using 632.8-nm and 442-nm laser line excitations to probe the electronic properties in the bulk of the nc-Si:H intrinsic layer and the top layer near the *i/p* interface, respectively. The PL spectra were plotted in Fig. 2 for comparison with the Raman results.

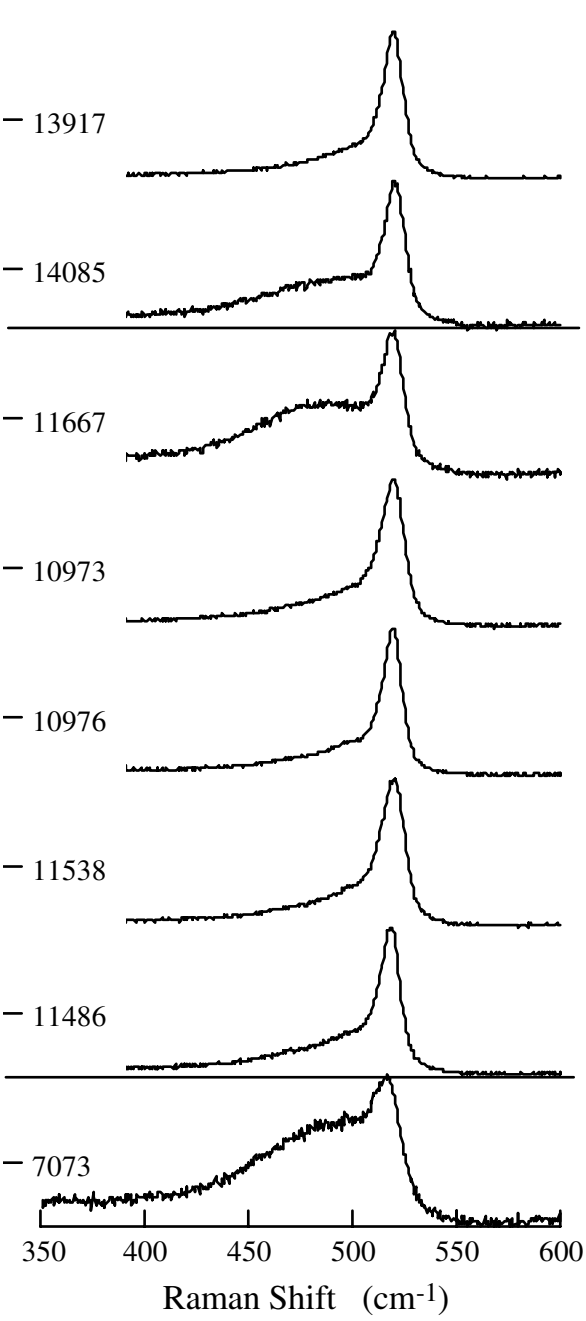

Figure 1. Raman spectra of the eight nc-Si:H solar cells.

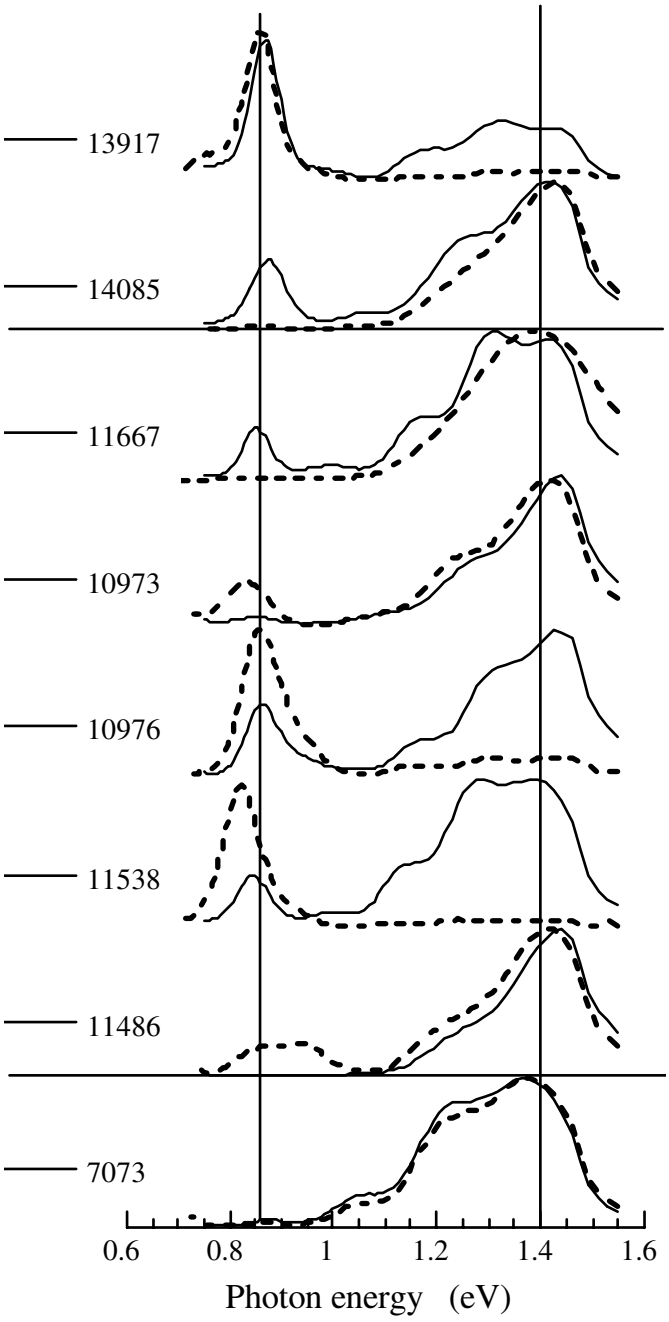

Figure 2. PL spectra of the same nc-Si:H solar cells at 80 K excited by 632.8-nm (solid) and 442-nm (dashed) laser beams.

Table II. Summary of the Raman and PL analyses of the nc-Si:H solar cells.

Dep. method	Sample ID#	f_c (%)	$f_{g.b}$ (%)	$I_{PLc}/(I_{PLc}+I_{PLa})$		T_L (K), 633 nm		T_L (K), 442 nm	
				633 nm	442 nm	nc-peak.	a-peak	nc-peak.	a-peak
RF	13917	80.6	35.8	68.7	92.8	19.3	17.4.	17.8	-
	14085	53.4	13.1	32.5	3.4	20.7	21.7	22.0	18.1
VHF	11667	40.4	5.0	26.3	2.1	21.7	23.7	20.2	15.2
	10973	74.8	30.8	5.1	24.1	15.6	21.1	15.2	-
	10976	79.0	34.5	32.9	87.0	19.9	23.3	18.7	-
	11538	77.8	34.5	25.1	95.0	17.8	23.0	16.7	-
	11486	72.2	31.1	1.0	18.5	31.2	21.5	22.2	-
μW	7073	37.6	14.5	4.0	3.7	36.9	22.8	29.1	-

where f_c, and $f_{g.b.}$ are the total nanocrystalline volume fraction included in the grains and the grain boundaries and the grain boundary volume fraction calculated from Raman spectra, respectively, $I_{PLc}/(I_{PLc}+I_{PLa})$ the fraction of the nanocrystalline PL intensity, and T_L the characteristic temperature of PL as described in the text.

The Raman spectra of nc-Si:H can be decomposed into three components, a sharp Lorentzian peak at 520 cm^{-1} corresponding to the scatterings from nanocrystalline grains, a smaller Gaussian peak at 490-500 cm^{-1} assigned to the scatterings from grain boundaries, and a broad Gaussian peak at 480 cm^{-1} corresponding to the amorphous component. From the decomposition of Raman spectra, we deduced the total nanocrystalline volume fraction (f_c) and the grain boundary volume fraction ($f_{g.b.}$) using our earlier publications [7,8]

$$f_c = (I_c + I_{gb})/[I_c + I_{gb} + y(L)I_a], \quad (1)$$

$$f_{g.b} = I_{gb}/[I_c + I_{gb} + y(L)I_a], \quad (2)$$

where I_c, I_{gb} and I_a are the integrated intensities of the peaks associated with the nanocrystalline grain, grain boundary, and amorphous components, respectively. $y(L) = 0.8$ for the grain size of $(L) \sim 10$ nm is used [7,9]. Table II lists the calculated f_c and $f_{g.b.}$ values from Fig.1.

As shown in Fig. 2, most of the nc-Si:H solar cells show two separated PL peaks at 80 K. The broad peak at ~1.4 eV originates from the tail-to-tail radiative recombination in the a-Si:H region, while the narrow peak at ≤ 0.9 eV is related to the nanocrystalline grains and from the tail-to-tail radiative recombination in the grain boundary regions [7,9-11]. The relative PL intensity of the grain boundary region is represented by the fraction of $I_{PLc}/(I_{PLc}+I_{PLa})$, where I_{PLc} and I_{Pla} are the integrals of the low and high energy PL peaks, respectively. One finds that $I_{PLc}/(I_{PLc}+I_{PLa})$ using 442-nm excitation change in the same manner as $f_{g.b.}$ does. Furthermore, the width of the electronic band tails, kT_o, could be obtained from the temperature dependence of the corresponding PL intensities. According to the carrier thermalization model, $kT_o = kT_L \ln(\nu_o \tau_r)$, where T_L, ν_o, and τ_r are the slope of I_{PL}-T plot, the attempt-to-escape frequency, and the carrier's recombination lifetime, respectively [11]. The T_L can be deduced by fitting the experimental data into $I_{PL} = I_o \exp(-T/T_L)$. Table II also summarizes the analysis of PL data for the eight nc-Si:H cells.

DISCUSSION

We first compare the two nc-Si:H cells deposited using RF glow discharge. The main difference is that the sample 13917 was deposited using a constant hydrogen dilution, while the sample 14085 using a profiled hydrogen dilution with decreasing hydrogen dilution during the deposition. As shown in Table I, the hydrogen dilution technique has improved V_{oc} and FF significantly, but there is a slight loss in the J_{sc}. A recent study using the hydrogen dilution profiling technique has resulted in an efficiency of 8.4% of the nc-Si:H single-junction cell and 13.4% of a-Si:H/nc-Si:H double-junction cell [13]. Raman results indicate that sample 14085 has much lower crystalline volume fraction than sample 13917, which is consistent with the observed higher V_{oc} and lower J_{sc} in the profiled cell than in the flat one. However, we need to keep in mind that the Raman measurement with 514.5-nm excitation only detects the top layer near the *i/p* interface. The crystalline volume fraction may be over-estimated for the sample with flat hydrogen dilution, but under-estimated for the sample with the profiled hydrogen. Another interesting observation is that the grain boundary volume fraction is relatively lower in the sample 14085 than in the sample 13917, which implies that a low percentage of grain boundary is desirable for solar cell performance. Meanwhile, the hydrogen dilution profiling (#14085) results in a clear difference of the electronic density of states in the top layer from the bulk as shown in the PL spectra, i.e. the amorphous-related peak dominants and the nanocrystalline-related peak diminishes when the excitation was changed from the long wavelength (632.8-nm) to the short wavelength (442-nm). This is opposite to the samples with flat hydrogen dilution (#13917), where the nanocrystalline-related peak increases at the top layer.

The MVHF deposited nc-Si:H cells (#11667) with a thick a-Si:H *i/p* buffer layer showed an improved cell performance due to reduced shunt current as described in our previous paper [6]. Raman measurement showed a low crystalline volume fraction with very little of grain boundary component and PL showed a low nanocrystalline related peak at the *i/p* interface layer. Both results are consistent with the expected effect of the a-Si:H buffer layer.

As reported previously [6], we found that some unoptimized nc-Si:H solar cells showed a significant ambient degradation related to post-oxidization. Cells 10973 and 10976 are made under two conditions such that one produces no ambient degradation and the other one does. Raman results show that sample 10976 has slightly high f_c, whereas, PL spectra are very different. Sample 10976 has a much higher nanocrystalline related PL peak than sample 10973, especially, at the top layer, indicating a high non-uniformity along the growth direction [13]. It has been showed that a high nanocrystalline volume fraction with large grains easily causes micro-cracks [14], post-oxidization, and consequently the ambient degradation.

Now we discuss the band tail width deduced from PL temperature dependence. As listed in table II, the T_L related to the amorphous PL peak is in the range from 17 to 23 K for all the eight cells in the bulk (632-nm excitation), and in the top layer (442-nm excitation) T_L is ~ 17±2 K for the two high efficiency cells. The T_L for the nanocrystalline related PL peak could be categorized into two types. In the cells with reasonable performance, the T_L is smaller than 23 K and changes very little from the bulk to the top layer. In contrast, in the high rate MVHF (#11486) and the microwave cell (#7073) have large T_L values (31-37 K) in the bulk. Since the band tail width kT_o is proportional to T_L, the large T_L in the poor nc-Si:H solar cells implies that a broad band tail in the nanocrystalline region leads to a poor cell performance. Normally, the band tail in the nanocrystalline region is considered from the grain boundary states. Therefore, finding ways to improve the grain boundary quality (less defects and less distorted bonds) would be beneficial for improving the nc-Si:H solar cell performance.

SUMMARY

The Raman results show that a high f_c leads to a high J_{sc} and low V_{oc} in nc-Si:H solar cells made with constant hydrogen dilution. f_c increases as film grows for flat hydrogen dilution [13]. However, hydrogen dilution profiling, with dilution decreasing as film grows, lowers f_c as measured by 514-nm light with a penetration depth of 60 nm. The PL spectra excited by 632-nm and 442-nm laser beams indicate that the crystallinity increased along the growth direction for the flat hydrogen diluted samples. The top layers in the hydrogen dilution profiled nc-Si:H cells, however, have a higher amorphous PL signal than in the bulk. The improved cell efficiency by hydrogen dilution profiling indicates that a properly controlled f_c distribution along the growth direction is a very useful technique to obtain high efficiency. The band tail width in the grain boundary region was deduced from the PL intensity temperature dependence. The results show that a narrow band tail in the nanocrystalline phase correlates to improved cell efficiency.

ACKNOWLEDGMENT

This work is supported by NREL Thin-Film partnership program Subcontract No. ADJ-1-30630-09 at University of North Carolina and ZDJ-2-30630-19 at United Solar Ovonic Corporation. The authors thank J. Owens for critical reading.

REFERENCE

1. J. Yang, A. Banerjee, and S. Guha, *Appl. Phys. Lett*. **70**, 2975 (1997).
2. A. Banerjee, J. Yang, and S. Guha, *MRS Symp. Proc*. **557**, 743 (1999).
3. J. Meier, P. Torres, R. Platz, S. Dubail, U. Kroll, J. A. Anna Selvan, N. Pellaton Vaucher, Ch. Hof, D. Fischer, H. Keppner, A. Shah, K.-D. Ufert, P. Giannoules, and J. Koehler, *MRS Symp. Proc*. **420**, 3 (1996).
4. K. Ogawa, K. Saito, M. Sano, and A. Sakai, *in Technical Digest of International PVSEC-12*, 2001 Jeju, Korea, pp. 343-346.
5. K. Yamamoto, M. Yoshimi, Y. Tawada, S. Fukuda, T. Sawada, T. Meguro, H. Takata, T. Suezaki, Y. Koi, K. Hayashi, T. Suzuki, and A. Nakajima, *in Technical Digest of International PVSEC-12*, 2001 Jeju, Korea, pp. 547-548.
6. B. Yan, G. Yue, J. Yang, A. Banerjee, and S. Guha, *MRS Symp. Proc*. **762**, 309 (2003).
7. Guozhen Yue, J. D. Lorentzen, Jing Lin, Qi Wang and Daxing Han, Appl. Phys. Lett. **75**, 492-494 (1999).
8. Daxing Han, J. D. Lorentzen, J. Weinberg-Wolf, L. E. McNeil, and Qi Wang, J. Appl. Phys., **94**, 5 (2003) 2930-2936.
9. C. Droz, E. Vallat-Sauvain, J. Bailat, L. Feitknecht, J. Meier, X. Niquille, A. Shah, Proceedings of 3rd World conference on PV Energy Conversion, Osaka Japan, (2003).
10. Daxing Han, Guozhen Yue, J. D. Lorentzen, Jing Lin, H. Habuchi, and Qi Wang, J.Appl. Phys. **87(4)**, 1882-1888 (2000).
11. Daxing Han and Keda Wang, Solar Energy Materials and Solar Cells, **78** (2003) 181-233.
12. R. Carius, T. Merdzhanova, F. Finger, , *MRS Symp. Proc*. **762**, 321 (2003).
13. B. Yan, G. Yue, J. Yang, S. Guha, D. Han, D. L. Williamson, and C.-S. Jinag, *MRS Symp. Proc*. **808**, A8.5 (2004), in press.
14. F. Finger, S. Klein, T. Dylla, A. L. Baia Neto, O. Vetter, and R. Carius, Mat. Res. Symp. Proc. **715**, 213 (2002).